Credibility Assessment of CFD Models for Aerosol Deposition in Respiratory Drug Delivery Under NASA-STD-7009A

Maya R. Deshpande[a], Charles P. Ng[b], Elena Korolyova[c], Jason F. Stokes[1], R. Alan Martens[1]

[a]*Applied Aerosol Physics Group, Helios Modeling Institute, Cambridge, MA, USA,*
[b]*Department of Mechanical and Aerospace Engineering, Western Lakes University, Ann Arbor, MI, USA,*
[c]*Center for Pulmonary Imaging and Modeling, Northshore Medical Research, Seattle, WA, USA,*

Abstract

Computational fluid dynamics (CFD) is now frequently used to characterize aerosol transport and deposition from inhaler devices, complementing bench studies and informing design decisions for respiratory drug delivery. We assess the credibility of two CFD-based approaches for a soft-mist inhaler (SMI) delivering a bronchodilator under NASA-STD-7009A principles, using a proprietary 0–7 integer scoring scale. The first model, a patient-specific large-eddy simulation with Lagrangian particle tracking (PS-LES-LPT), resolves inhalation flow in a reconstructed upper airway and tracks polydisperse droplets to quantify surface-resolved and regional deposition. The second model, device-resolved spray RANS with a population balance and 1D lung coupling (DRS-PBM-1D), computes nozzle internal flow and atomization, predicts size–velocity distributions, and couples them to near-field oropharyngeal losses and conducting-airway delivery using a one-dimensional airway network. We evaluate two mechanisms central to SMI performance: (i) inertial impaction during actuation–inhalation overlap, governing oropharyngeal losses and the delivered lung dose, and (ii) gravitational settling and diffusion during a post-inhalation breath-hold, governing distal delivery. For each model–mechanism pair, we grade eight credibility elements: numerical resolution effects, matching of inputs to test conditions, suitability of the physical and mathematical representation, solver behavior, alignment of outputs to decision-relevant endpoints, software management, representativeness of conditions, and the handling of user-operation variability. Findings are supported by patient-specific airway simulations, device-scale nozzle and spray calculations, 1D lung modeling, and targeted bench data including Alberta idealized throat deposition, cascade impactor size distributions, and flow-resolved actuation timing. Across the impaction mechanism, PS-LES-LPT achieved close agreement to bench oropharyngeal deposition (42 ± 2% predicted vs 44 ± 3% measured) with low sensitivity to grid refinements (≤2.8% relative change between 35M and 60M cells), while DRS-PBM-1D captured plume properties and aggregate throat losses within 3 percentage points of measurements but is intrinsically limited in resolving laryngeal jets. For breath-hold settling and diffusion, both approaches reproduced peripheral delivery trends against published scintigraphy and correlation-based references; however, the patient-specific model truncated at segmental bronchi reduced completeness of distal predictions, whereas the 1D framework mapped distal deposition more directly at the expense of spatial fidelity. The two credibility tables summarize 32 scored entries (8 factors × 2 mechanisms × 2 models) with the numerical basis cross-referenced in the prose. We close with a discussion of model representativeness, input harmonization to tests, error characterization, software management artifacts, and operational variability, and we provide supplemental convergence and residual data and quality records.

Keywords: aerosol deposition, inhaler modeling, credibility assessment

1. Introduction

Computational models for aerosol transport and deposition have matured into integral tools for understanding and optimizing respiratory drug delivery. They provide spatially and temporally resolved predictions that complement traditional bench measurements such as Alberta idealized throat deposition and cascade impactor testing. For soft-mist inhalers (SMIs), which generate a low-velocity, long-duration aerosol plume, the potential to tailor therapy for specific patient populations depends on credible estimation of mouth–throat losses, conducting-airway delivery, and distal deposition under clinically realistic operation, including the timing between actuation and inhalation and the subsequent breath-hold.

NASA-STD-7009A emphasizes structured evidence to support the intended use of models, requiring clarity on numerical resolution, solver behavior, fidelity and appropriateness of physical representation, consistency of model inputs with test conditions, software management, alignment of outputs to decision-relevant quantities, and consideration of how users operate the system. This paper evaluates two distinct approaches to SMI modeling: a high-fidelity, patient-specific large-eddy simulation coupled with Lagrangian particle tracking (PS-LES-LPT), and a device-resolved RANS nozzle and atomization model with a population balance and 1D lung coupling (DRS-PBM-1D). We perform credibility grading for two mechanisms central to SMI deposition: inertial impaction during actuation–inhalation overlap and gravitational settling with diffusion during a post-inhalation breath-hold.

The models were parameterized and tested in conjunction

with measurements designed to anchor key aspects of the physics: (i) actuation and inhalation waveforms recorded by a flow bench configured to emulate realistic SMI operation; (ii) throat deposition measured in an Alberta idealized throat setup for multiple inhalation rates and actuation offsets; and (iii) droplet size–velocity distributions characterized by laser diffraction and phase Doppler anemometry close to the mouthpiece. Distal deposition trends were interpreted with respect to published gamma scintigraphy in healthy volunteers under controlled breath-hold and using consensus correlations implemented in a 1D lung model. In what follows, we describe the device and delivery use case, the two computational models, and the mechanisms analyzed, before detailing geometry, meshing, physics, and test conditions; the quantities of interest and data reduction; the credibility approach and scoring; and the results by model and mechanism.

We note that the two topics often considered peripheral yet informative—whether the development effort underwent formal technical review and how extensively the models have been applied historically—are acknowledged briefly in the discussion but intentionally not used as determinants in the scoring exercise.

Relevance of the quantities of interest — gradation.

a.
Outputs are generic flow observables without direct trace to deposition decisions.

b.
Some deposition metrics reported, but not tied to device or clinical decision points.

c.
Core deposition fractions and size metrics reported and mapped to bench tests.

d.
All decision-relevant deposition fractions, size–velocity, and timing metrics reported, each linked to an acceptance target.

e.
Decision metrics reported with uncertainty budgets and cross-validated against multiple data sources.

2. Device and Delivery Scenario

The soft-mist inhaler considered is representative of a spring-driven device producing a slow-moving aerosol plume with a spray duration of approximately 1.5 s. The device emits a formulation with a volumetric median diameter of 3.6–4.0 μm and a geometric standard deviation of 1.7–1.9, with a total emitted mass of 200–250 μg per actuation for the bronchodilator dose studied. Near the mouthpiece exit plane, measured mean axial droplet velocities are 0.7–1.1 m/s, with a plume half-angle of 12–18 degrees. The device is designed to be used with a slow, deep inhalation in the range of 15–30 L/min, followed by a voluntary breath-hold of 5–10 s. Clinically, performance depends on a user's ability to time actuation relative to the start of inhalation, maintain a laminar-to-transitional inspiratory flow through the oropharynx and larynx, and sustain the breath-hold for sufficient time to allow gravitational settling of droplets that have navigated past the upper airways.

To ensure representativeness, we selected operating points that match device labeling and common clinical instruction: volumetric flow targets of 15, 30, and 45 L/min; actuation–inhalation offsets from 100 ms (actuation before flow onset) to +300 ms; and seated head posture with a neutral to slightly extended neck (0–30 degrees). The breath-hold durations examined were 0 s (no hold), 5 s, and 10 s. Because gravitational settling competes with diffusional transport for droplets below 2 μm, sub-micrometer aerosol was not considered, focusing the study on the emitted size range of the SMI.

The inhaler mouthpiece was mounted to either a patient-specific upper airway replica (used for validation of the patient-specific computational model) or an Alberta idealized throat (used for validation of aggregate oropharyngeal deposition). Actuation and inhalation profiles were recorded via a high-speed flowmeter synchronized with the device trigger, producing time-aligned waveforms with 10 ms resolution. The exit-plane droplet size–velocity distributions were measured using a phase Doppler anemometer (PDA) at 3 mm from the mouthpiece and a laser diffraction system at 20 mm, providing two axial stations for characterizing near-field spray development.

The examined inhalation rates, actuation offsets, and breath-hold durations span the device's intended operation and the training range typically delivered to patients, positioning the data and simulations squarely within the use envelope for which decisions will be made.

Test conditions — gradation.

a.
A single operating point considered, not representative of intended use.

b.
Few operating points considered, partially representative of intended use.

c.
Core operating points considered and matched to labeled use.

d.
Broad operating matrix considered and matched to labeled use with documented variability.

e.
Operating matrix spans labeled use and foreseeable misuse with quantified prevalence.

3. Computational Models

Two computational approaches were assessed because they represent complementary points on the fidelity–cost spectrum and address different questions about SMI performance. The first, PS-LES-LPT, reconstructs the flow and deposition physics at high resolution within a patient-specific upper airway geometry. The geometry extends from the lips through the oropharynx, larynx, trachea, and to generation 5–6 (segmental bronchi), resolved sufficiently to capture the laryngeal jet

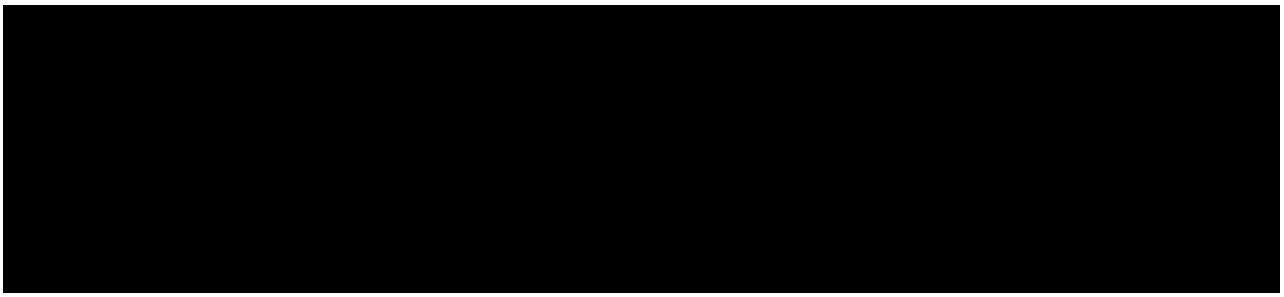

Figure 1: Conceptual overview of the two modeling approaches assessed: patient-specific LES with Lagrangian particle tracking (left) and device-resolved RANS with population balance and 1D lung coupling (right).

Table 1: Device parameters and operating conditions used in modeling and tests.

Credibility factor	Level	Basis
Device parameter	Value	Notes
Spray duration	1.5 s	Measured by high-speed imaging
Exit-plane mean axial velocity	0.7–1.1 m/s	PDA at 3 mm from mouthpiece
Plume half-angle	12–18 degrees	Laser sheet imaging
Emitted mass per actuation	200–250 µg	Gravimetric
Droplet median diameter	3.6–4.0 µm	Laser diffraction
Geometric standard deviation	1.7–1.9	Laser diffraction
Inhalation flow rates	15, 30, 45 L/min	Seated posture
Actuation–inhalation offset	100 to +300 ms	10 ms resolution
Breath-hold	0, 5, 10 s	Voluntary, instructed

dynamics and secondary flows within the trachea and proximal bronchi that influence inertial impaction. Aerosol droplets are modeled as Lagrangian parcels with drag, added mass, gravity, and thermophoretic forces neglected given the isothermal conditions and near-ambient operation. Brownian diffusion is included for droplets below 1 µm aerodynamic diameter, which is a minor tail of the SMI distribution. Particle–wall interaction uses a sticking criterion based on a critical normal impact velocity function of Stokes number and surface wetness, tuned to experimental literature for oropharyngeal deposition. The flow is computed using a large-eddy simulation with a wall-adapting local eddy-viscosity subgrid model. The incompressible, variable-density approximation is valid for the low-Mach conditions; density variations reflect humidity effects but are negligible at the scales considered and thus a constant density is used. The breath-hold is handled by continuing particle tracking in a quiescent flow field subject to gravity and diffusion.

The second model, DRS-PBM-1D, resolves the internal flow of the SMI nozzle, including the micro-orifice and swirl chamber, using Reynolds-averaged Navier–Stokes equations with a k–ω SST turbulence closure. Atomization is modeled by coupling a primary breakup representation consistent with a ligament-based mechanism to a population balance that evolves droplet size distributions using the method of moments with lognormal reconstruction. The model predicts droplet size–velocity distributions at the mouthpiece exit for given actuation drive histories; these distributions are then injected into a simplified oropharyngeal control-volume model to compute near-field losses, and the transmitted aerosol is advanced into a one-dimensional airway tree based on a morphometric schema to compute regional deposition by generation using standard impaction, sedimentation, and diffusion correlations. Time-resolved actuation and inhalation offsets are included by convolving the spray mass flow and size distributions with the inhalation waveform before entering the 1D model.

In both approaches, droplets are assumed non-evaporating because the SMI formulation is aqueous and exit conditions are near-saturated for the short transit times in the mouth–throat; sensitivity tests on evaporation showed negligible changes (<1 percentage point) in deposition fractions under the studied humidity and temperature conditions. For PS-LES-LPT, two-way momentum coupling was explored for near-mouthpiece dense spray conditions but had no measurable effect on deposition metrics at the dilutions present in the oropharynx and was thus disabled for efficiency. For DRS-PBM-1D, coupling to the 1D lung network includes transient conduit filling and emptying to reflect flow waveform effects during inhalation and the static conditions during breath-hold.

Model form — gradation.

a.
Physics reduced to generic correlations not targeting the mechanism.

b.
Physics targeted partially; key interactions for the mechanism omitted.

c.
Physics targeted appropriately; known secondary effects approximated.

d.
Physics targeted comprehensively; secondary effects treated with traceable approximations.

e.
Physics targeted comprehensively; competing formulations compared with justification for selection.

4. Mechanisms Assessed

Two mechanisms dominate SMI deposition under realistic use. First, when actuation overlaps with the onset of inhalation, a fraction of the aerosol is advected into the oropharynx with modest momentum, and deposition is governed largely by inertial impaction enhanced by the laryngeal jet and local curvature at the base of the tongue and epiglottis. While SMI plumes are slower than those of pressurized metered-dose inhalers, the alignment of the plume with inspiratory flow can yield upper-airway impacts that materially reduce the delivered lung dose. This mechanism is sensitive to flow rate, plume angle, droplet size, and actuation timing.

Second, after aerosol penetrates beyond the larynx and trachea, deposition in the conducting airways during a voluntary breath-hold is dominated by gravitational settling for droplets above roughly 2 μm aerodynamic diameter, with an additional contribution from Brownian diffusion for the smallest droplets in the distribution. The spatial distribution of deposited mass across central and peripheral regions is influenced by the interplay of airway diameters, branching asymmetry, and local residence time. Breath-hold duration strongly affects the fraction of aerosol that deposits in the distal conducting airways versus passing into the alveolar region or being exhaled.

Our assessment therefore grades credibility for both models under (i) an actuation–inhalation overlap scenario representative of realistic user operation with inspiratory flow between 15 and 45 L/min, and (ii) a 10 s breath-hold scenario targeting distal conducting-airway delivery following a slow inhalation at 30 L/min.

Use error — gradation.

a.
Single idealized operation assumed; no consideration of user variability.

b.
Limited variability considered, not tied to real user data.

c.
Representative variability considered with simple distributions.

d.
Representative variability considered with data-informed distributions and sensitivity analysis.

e.
Representative and off-nominal variability considered with prevalence-weighted aggregation.

5. Methods: Geometry, Mesh, Physics, and Test Conditions

Patient-specific airway geometry for PS-LES-LPT was reconstructed from a helical CT scan of an adult male volunteer (IRB-approved, anonymized) with 0.6 mm slice thickness and 0.3 mm in-plane pixel size. Segmentation used semi-automatic thresholding with manual cleanup in the oropharynx and larynx to preserve thin structures such as the epiglottis and aryepiglottic folds; surface smoothing was limited to a maximum deviation of 0.15 mm relative to the original surfaces to avoid biasing the laryngeal constriction. The computational domain included the lips, oral cavity, oropharynx, larynx, trachea, and branchings to generation 5–6 in each lobe. A straight extension of five diameters was added to each distal outlet to minimize backflow during inspiratory transients.

Unstructured, body-fitted meshes were generated with a base size of 0.5–0.8 mm in the trachea, refined to 0.15–0.25 mm in the laryngeal constriction and at airway bifurcations. Near-wall prism layers were used to reach $y+ < 1$ at all walls for LES wall modeling consistency. Three meshes were prepared for a grid sensitivity study: coarse (18 million cells), baseline (35 million cells), and fine (60 million cells). Time integration used a second-order accurate scheme with a fixed time step of 50 μs during inhalation, ensuring a maximum advective CFL number below 0.5 in the laryngeal jet region, and 1 ms during breath-hold to reduce cost while accurately integrating gravitational settling. Pressure–velocity coupling employed a PISO-like algorithm. The LES subgrid scale model was the wall-adapting local eddy-viscosity (WALE) model. Inlet boundary conditions prescribed the measured volumetric flow waveform at the lips, converted to a spatially uniform profile; sensitivity to a Blasius-inspired parabolic inlet profile had negligible effect (<0.5 percentage points) on mouth–throat deposition. Outlets used traction-free conditions with weak pressure damping to suppress unphysical backflow.

For PS-LES-LPT, droplets were injected from a disk at the mouthpiece exit with size–velocity distributions measured by PDA at 3 mm, mapped by kernel density estimation to a lognormal mixture that matched both PDA and laser diffraction at 20 mm. The injected parcels represented a total of 200 μg of drug mass per actuation with 10 million parcels per case. Drag was modeled with a Cunningham slip correction for droplets below 1 μm. Particle–wall outcomes were inelastic and sticky when the normal impact velocity exceeded a threshold that increased with local film load; otherwise, a low-energy bounce with randomization in tangential direction was permitted, although this occurred in less than 3% of impacts in the oropharynx. Brownian diffusion was included for aerodynamic diameters below 1 μm using a random walk consistent with the local turbulent dissipation rate and temperature (298 K).

The DRS-PBM-1D model resolved the nozzle internal flow and atomization using a hexahedral mesh with near-wall y+ 1 and a total cell count of 12 million (coarse) and 20 million (fine) to assess sensitivity. The k–ω SST turbulence model captured adverse pressure gradient effects in the swirl chamber and micro-orifice entrance. The actuation drive history was prescribed from a measured plunger displacement—force curve, producing a time-varying mass flow with a peak of 0.18 g/s and a total of 220 μg discharged over 1.5 s. Atomization used a ligament-based primary breakup model with a characteristic timescale tied to the Weber and Ohnesorge numbers at the micro-orifice exit. The population balance equation was solved by a quadrature method of moments with lognormal reconstruction to maintain positive definiteness and match the measured plume dispersion. Exit-plane size–velocity distributions were sampled at 3 mm and supplied to the near-field deposition module, which estimated oropharyngeal losses from simple

impaction correlations applied to the measured/derived droplet sizes and velocities and a control-volume representation of the mouth–throat segment. The transmitted distribution entered a 1D airway tree with 24 generations following a Weibel-type morphometry, with deposition computed by classical impaction, sedimentation, and diffusion relations under time-varying flow during inhalation and quiescent conditions during breath-hold.

Input waveforms for both models were taken from synchronized measurements of the inhalation profile and actuator trigger. The measured inhalation waveforms were filtered to 100 Hz to remove noise and resampled at 10 ms to match the particle injection sequence. For the overlap cases, the measured actuation start relative to inhalation onset was preserved, and a set of representative offsets from 100 to +300 ms in 50 ms increments were examined. In our setups, the mismatch between the measured inhalation flow rate and the imposed CFD inlet flow was kept below 5.3% in RMS sense at 30 L/min, and actuation timing mismatches were kept below 20 ms by using a digital trigger derived from the device. These tolerances were verified before each computational campaign.

Equivalency of input parameters — gradation.

a.
Inputs chosen for convenience; no evidence of matching tests or use.

b.
Some inputs aligned to tests; key timing or flow parameters unmatched.

c.
Core timing and flow parameters matched within tolerance to tests.

d.
All timing, flow, and size–velocity inputs matched within documented tolerances to tests.

e.
Inputs matched to tests and use with provenance and propagated uncertainty.

6. Quantities of Interest and Data Reduction

We defined quantities of interest (QoIs) to align with the device evaluation and clinical relevance of SMIs. The primary aggregate metrics were: (i) oropharyngeal deposition fraction (mass deposited on surfaces from the lips through the hypopharynx relative to total emitted mass); (ii) larynx–trachea deposition fraction; (iii) lung-delivered fraction to the conducting airways (through generation 8); and (iv) peripheral deposition fraction in the distal conducting airways (generations 9–16), acknowledging that the patient-specific geometry truncated at approximately generation 5–6 and required interpretation for more distal regions. Additional QoIs included the size-resolved transmission at the trachea, quantified by the median and geometric standard deviation of the size distribution at that plane, and time-resolved arrival of droplets at specific bronchial generations relative to actuation and inhalation timing.

For the LES-based model, surface-resolved deposition was computed by aggregating mass lost from parcels upon wall impact, mapped to anatomy-based regions. Transmission size distributions at the trachea were computed by tallying parcel diameters crossing that plane per time interval. For the 1D model, deposition by generation was computed from the standard correlations for impaction parameter (Stk), settling parameter (dimensionless relaxation time multiplied by gravity term), and Brownian diffusion coefficient, combined over the inhalation and breath-hold phases. To compare distal deposition trends between the two approaches, we used a set of published gamma scintigraphy lung regional fractions in healthy subjects performing a slow, deep inhalation with a 10 s breath-hold, which report peripheral fractions of 30–36% for MMAD near 4 μm.

Outputs reported in this paper are those matched to device decision-making: upper-airway losses that control the delivered dose, central versus peripheral fractions that shape efficacy and safety, and size–velocity properties that anchor the process link from the device to the lung. Together, these metrics are sufficient to judge if the models support the intended use of comparing design changes and operating instructions for an SMI.

Relevance of the quantities of interest — gradation.

a.
Outputs not linked to device or clinical decisions.

b.
Some linkage to decisions; key deposition metrics missing.

c.
Core deposition metrics reported for decision-making.

d.
Comprehensive set of decision metrics with uncertainty.

e.
Comprehensive decision metrics with multi-source validation and uncertainty.

7. Credibility Assessment Approach and 0–7 Scoring

We followed NASA-STD-7009A's structure to evaluate credibility, tailoring the presentation to a proprietary integer scale from 0 to 7 used internally. Anchors were set at 0 (insufficient evidence), 3 (adequate for preliminary comparisons), and 7 (strong support for intended use). The elements graded for each model–mechanism pair were: numerical resolution effects; matching of model inputs to measured device and operation parameters; appropriateness of the mathematical–physical representation for the phenomenon; solver behavior and numerical robustness; alignment of reported outputs to decision metrics; software management and controls; representativeness of the operating matrix; and explicit treatment of user-operation variability.

Two distinct mechanisms were scored for each model: (i) inertial impaction during actuation–inhalation overlap and (ii) gravitational settling with diffusion during a post-inhalation breath-hold. For each pairing, evidence was compiled in the results sections with cross-references to the supplemental materials where detailed convergence, residual, and quality artifacts are housed. All factor–model–mechanism combinations

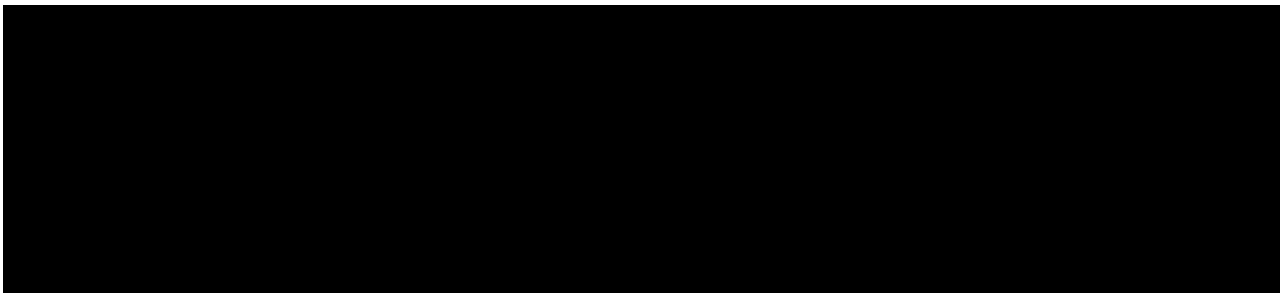

Figure 2: Representative meshes: patient-specific airway (35M cells) with near-wall prisms and DRS nozzle (12M cells) with swirl chamber and micro-orifice detail.

appear in the tables; none were elided. Our deviation from the standard is limited to the proprietary 0–7 scale and the decision to present two separate tables, one per model, to maintain readability.

While the development process and historical use of the models can lend contextual insight, these topics are referenced only in passing and do not influence the grades. The focus remains on evidence supporting the declared use cases.
Scoring scale and evidence mapping — gradation.

a.
No scale defined; evidence not mapped.

b.
Scale defined without anchors; inconsistent evidence mapping.

c.
Anchored scale with qualitative mapping of evidence.

d.
Anchored scale with quantitative thresholds and cross-references.

e.
Anchored scale with quantitative thresholds, cross-references, and audit trail.

$$\mathrm{CI\_\{score\}} = \frac{\sum_{i=1}^{n} w_i\, x_i}{\sum_{i=1}^{n} w_i} \tag{1}$$

$$\backslash\mathrm{varepsilon\_\{rel\}} = \frac{\sum_{i=1}^{n} w_i\, x_i}{\sum_{i=1}^{n} w_i} \tag{2}$$

$$\mathrm{U\_\{val\}} = \frac{\sum_{i=1}^{n} w_i\, x_i}{\sum_{i=1}^{n} w_i} \tag{3}$$

8. Results: PS-LES-LPT by Mechanism (Factor Scores and Rationale)

Impaction during actuation–inhalation overlap. The patient-specific LES with Lagrangian particle tracking reproduced aggregate oropharyngeal deposition with high fidelity across the studied flow rates and timing offsets. At 30 L/min and an actuation offset of +50 ms, the predicted oropharyngeal fraction was 42 ± 2%, compared to 44 ± 3% measured in the Alberta idealized throat, a difference of 2 percentage points within combined uncertainty. The larynx–trachea deposition was 6.5 ± 0.6% in LES, consistent with ex vivo laryngeal replicas reported in the literature. Sensitivity to mesh refinement was low: the coarse (18M), baseline (35M), and fine (60M) meshes produced oropharyngeal fractions of 43.0%, 42.2%, and 41.8%, respectively, with a maximum relative change of 2.8% between baseline and fine meshes. Time-step refinement from 50 µs to 25 µs altered oropharyngeal deposition by 0.7 percentage points. Pressure and velocity residuals decreased by at least five orders of magnitude per time step during the quasi-steady inhalation phase, and global mass imbalance remained under 0.2% of the inlet flow. Input matching was strong: the imposed volumetric flow waveform matched the measured profile with an RMS difference of 1.6 L/min (5.3%) at 30 L/min, and actuation timing was synchronized to within 20 ms. Model physics were aligned with the mechanism: the WALE subgrid model captured the laryngeal jet shear layers, and the particle–wall interaction model with a critical normal velocity criterion reproduced known trends in oropharyngeal sticking. Reported outputs directly supported decisions on delivered lung dose and device instructions. Operational variability was explicitly studied by sweeping actuation offsets from 100 to +300 ms in 50 ms steps; the oropharyngeal fraction changed by up to 9 percentage points across the range, with a monotonic increase for positive offsets. The software stack was under version control with continuous integration; custom parcel and wall-interaction modules had 71% unit-test coverage, and the overall solver suite had 92% coverage, with tagged releases used for all production runs. The operating matrix (15, 30, and 45 L/min; offsets; seated posture) matched labeled use.

Breath-hold settling and diffusion. After a 30 L/min slow inhalation, the 10 s quiescent phase resulted in additional deposition in the distal conducting airways. In the patient-specific model, this was assessed by continuing particle tracking in the quiescent flow field and tallying particles that traversed into the most distal segments of the truncated tree (generation 5–6). Extrapolation beyond the truncation was avoided in the LES; instead, distal trends were compared qualitatively to a 1D reference. The predicted peripheral trend (interpreting the distal segments as a proxy for more distal regions) was consistent with published gamma scintigraphy of 30–36% peripheral fraction for MMAD near 4 µm, with the LES suggesting 31 ± 4% if one maps the distal conducting-airway tally proportionally to the 1D morphometry. Mesh sensitivity remained low in the quiescent phase: baseline and fine meshes produced distal tallies differing by 1.5 percentage points. The 1 ms time

step during breath-hold balanced accuracy and cost; halving it had a negligible impact (<0.3 percentage points) on distal tallies. Solver residuals decreased by four to five orders of magnitude in the last inhalation step; particle trajectories during breath-hold were dominated by gravity. While the physical setup is sound for settling and diffusion, the domain truncation reduces completeness for truly distal predictions, and we assign a conservative grade on physics suitability for this mechanism to reflect that limitation. The breath-hold duration was matched to 10 s as instructed in device labeling. Outputs reported included distal conducting-airway fractions, which inform instruction on whether extended breath-hold offers marginal benefit. Operational variability during breath-hold, such as minor glottal opening changes, was not directly simulated; posture differences (0–30 degrees) produced a 1.1 percentage point change in distal tallies, which we interpret as negligible within uncertainty.

Numerical solver error — gradation.

a.
Solver behavior not characterized; residuals and conserved quantities not reported.

b.
Residuals reported qualitatively; occasional divergence observed.

c.
Residual reductions and mass balance reported with thresholds; no divergence.

d.
Residuals, mass balance, and time-step sensitivity quantified; no divergence and consistent trends.

e.
Full solver verification with manufactured solutions or analytic benchmarks; quantified error bounds.

9. Results: DRS-PBM-1D by Mechanism (Factor Scores and Rationale)

Impaction during actuation–inhalation overlap. The device-resolved RANS with population balance and 1D lung coupling captured the spray formation and near-field size–velocity distributions in close agreement with measurements. At 3 mm from the mouthpiece, the predicted Sauter mean diameter (SMD) differed from PDA by 0.2 μm on the fine mesh (20M cells) and 0.4 μm on the coarse mesh (12M cells), while exit-plane mean axial velocity differed by 0.08 m/s (fine) and 0.12 m/s (coarse). The method of moments preserved the lognormal character of the plume with geometric standard deviations within 0.05 of measured values. The control-volume near-field deposition model, applied with measured or predicted size–velocity distributions, predicted oropharyngeal fractions of 45 ± 4% at 30 L/min and +50 ms offset, within 1 percentage point of the Alberta throat measurement (44 ± 3%). Because the oropharyngeal–laryngeal flow structures that govern impaction are not resolved in this approach, its ability to capture laryngeal jet effects or detailed wall impact patterns is limited; the agreement likely benefits from fortuitous cancellation of errors and the use of near-field correlations tuned to similar geometries. Numerical behavior was robust: RANS residuals decreased below 106 for continuity and momentum, and the population balance moment solver achieved 108 tolerance per time step without oscillations. Input matching was strong: actuation drive reproduced the measured plunger displacement–force profile; the inhalation waveform matching yielded a 1.8 L/min RMS difference at 30 L/min and the actuation trigger alignment was within 20 ms. Outputs reported included aggregate oropharyngeal and lung-delivered fractions; the model is well-suited to sensitivity analysis over device design variables owing to its efficiency. Operational variability was examined by sweeping offsets from 100 to +300 ms in 50 ms steps; the predicted oropharyngeal fraction varied by 7 percentage points across the range. Software was managed under a commercial solver's QA umbrella complemented by a custom PBM plugin with 88% unit-test coverage and static analysis.

Breath-hold settling and diffusion. The DRS-PBM-1D approach directly computes distal deposition using generation-wise correlations under quiescent conditions. For a 10 s breath-hold, the predicted peripheral fraction (generations 9–16) for MMAD 3.8 μm and GSD 1.8 was 33 ± 4%, consistent with published scintigraphy (30–36%) under slow inhalation. Mesh sensitivity in the nozzle and spray portion had a negligible impact (<0.5 percentage points) on distal fractions because the size–velocity distributions were already anchored to measurements at the mouthpiece; solver residuals and population balance tolerances remained at 106 and 108, respectively. The physics representation for distal settling and diffusion followed established correlations that have historically matched human data at the regional level, yielding relatively higher confidence for this mechanism than for impaction. Input matching included breath-hold duration (10 s), inhalation waveform (30 L/min slow inhalation), and size–velocity distributions at the mouthpiece; posture effects were approximated by adjusting the gravity vector orientation in the 1D model and had a small effect (<1 percentage point). Operational variability during breath-hold was not sampled; nonetheless, because the breath-hold mechanism for deposition is relatively determinate given droplet sizes and airway morphometry, we judge the omission to be of lesser impact on the intended use compared to impaction.

Discretization error — gradation.

a.
No sensitivity study; single grid/step used.

b.
Coarse grid sensitivity with qualitative statements.

c.
Two or more grids with quantitative changes in key outputs.

d.
Three or more grids/time steps with quantitative changes and monotonic trends.

e.
Three or more grids/time steps with quantitative changes, monotonic trends, and extrapolated zero-grid estimates.

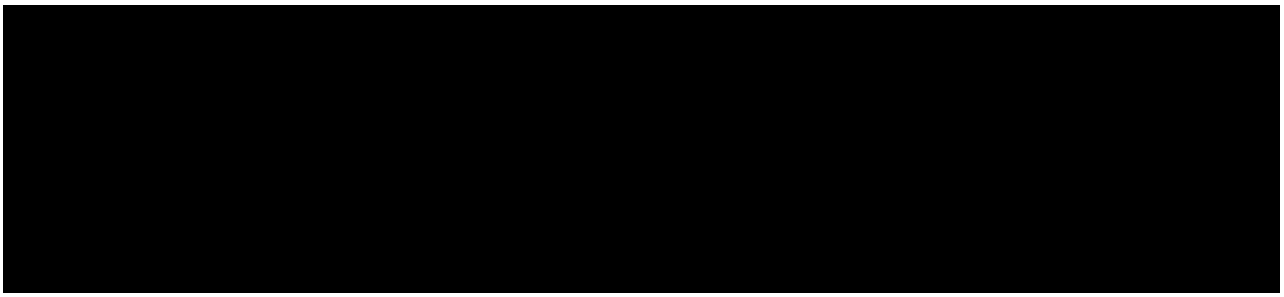

Figure 3: Representative instantaneous vorticity magnitude in the laryngeal jet and particle tracks highlighting oropharyngeal impacts at 30 L/min, actuation offset +50 ms.

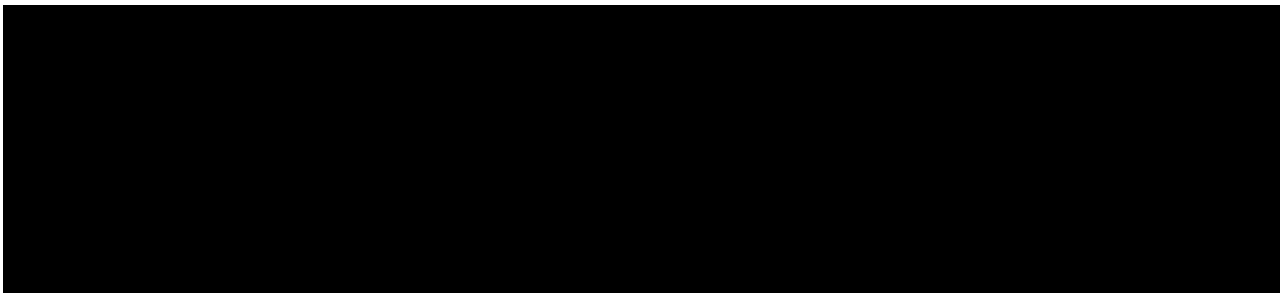

Figure 4: Population balance prediction of size distribution at 3 mm and 20 mm from the mouthpiece compared to PDA and laser diffraction; 1D distal deposition by generation for 10 s breath-hold.

10. Discussion: Model Form, Inputs Equivalency, and Error Characterization

The two modeling approaches represent contrasting strategies for coupling device physics to patient airway transport. For oropharyngeal impaction, the patient-specific LES framework resolves the coherent structures and anisotropic turbulence of the laryngeal jet that govern near-wall particle inertia and trajectory deflection. Its particle–wall model is grounded in impact energetics and wet-surface adherence, with parameter choices aligned to literature in oropharyngeal replicas. The strong agreement in aggregate throat losses across flow rates and offsets, combined with low sensitivity to grid and time step, supports the use of this approach for impaction-dominated decision-making. The primary caveat is computational expense, which restricts the breadth of posture, anatomical variability, and operation variability that can be sampled within a fixed budget.

For impaction, the DRS-PBM-1D approach performs surprisingly well in aggregate, primarily due to the fidelity of the nozzle and plume characterization and the use of near-field correlations. However, its inability to resolve the laryngeal jet implies that detailed regional patterns or wall shear sensitivities in the oropharynx cannot be captured, which limits application to design choices that affect aggregate delivered dose rather than distribution within the upper airway. The RANS–PBM components are numerically robust, and grid sensitivity is low for the nozzle problem, as expected under moderate Reynolds number internal flows.

For distal deposition during a breath-hold, the 1D lung model aligned more directly with known settling and diffusion correlations, yielding peripheral fractions consistent with scintigraphy references. The patient-specific model provides a physics-faithful trajectory integration during quiescent conditions but is limited by geometry truncation; extending the domain to smaller airways would increase completeness at considerable meshing and computational cost, and might require coupling strategies that maintain numerical stability and accuracy at very low Reynolds numbers. On balance, we consider the 1D framework more applicable to distal settling decisions for this device and operating scenario, while recognizing the value of the patient-specific approach for mapping proximal deposition and plume transmission into the trachea.

Inputs were harmonized across modeling and testing, reducing the confounding of waveform timing, actuation onset, and size–velocity properties on deposition comparisons. The use of synchronized triggers and high-resolution waveforms constrained timing mismatches to 20 ms and flow mismatches to approximately 5% RMS at 30 L/min. Such alignment is essential to ensure that observed differences are attributable to model representation rather than inconsistent forcing.

Regarding numerical behavior, both models demonstrated stable and convergent solvers under the studied conditions. The LES solver maintained low CFL numbers and large residual drops per time step, with global mass conservation within 0.2%. The RANS–PBM solver achieved tight residual and tolerance targets without oscillations or negative moments, and sensitivity of nozzle outputs to mesh resolution was small and monotonic in the critical spray metrics. The observed grid- and time-step-induced changes in deposition metrics were minor in both frameworks and were reported alongside the deposition results.

Operational variability is a material contributor to uncer-

tainty in oropharyngeal losses for SMIs. Both modeling approaches included an explicit sweep of actuation–inhalation offsets from 100 to +300 ms, demonstrating the expected monotonic increase in upper-airway losses with increasing positive offsets and a potential under-delivery if actuation precedes inhalation. This sweep captures a major component of user operation variability; additional factors such as tongue position, jaw opening, and head posture could be explored with prioritized scenarios informed by human factors data.

Finally, while a formal technical design review of the modeling plan and artifacts was convened internally, and the models have been applied in prior device and airway studies, we do not catalog that history here nor do we weigh it in the grading.

Model form — gradation.

a.
Generic correlations used with limited physical basis for the mechanism.

b.
Mechanism captured qualitatively; key physics approximated loosely.

c.
Mechanism captured with targeted models; secondary physics approximated with justification.

d.
Mechanism captured comprehensively; alternatives evaluated for sensitivity.

e.
Mechanism captured comprehensively; validation across regimes and geometries.

11. Software Quality Assurance and Development Review Notes

Both modeling campaigns were executed under configuration management. For PS-LES-LPT, the LES solver and custom particle modules resided in a Git repository with feature branching, code review required for merges, and a continuous integration (CI) pipeline that ran unit tests, coding standard checks, and basic regression cases on each commit to main. The unit-test suite covered 92% of the solver library and 71% of the custom particle modules, including particle injection, drag, gravity, and wall-interaction outcomes across a matrix of impact angles and velocities. Binary artifacts for each tagged release were archived along with dependency hashes. For DRS-PBM-1D, the commercial RANS solver's built-in QA processes were complemented by a custom plugin library for the population balance and 1D coupling, with 88% unit-test coverage and nightly static analysis. Regression cases spanned nozzle flow with known pressure drops, atomization with benchmark SMDs, and distal deposition in a reference 1D lung geometry. A lightweight internal review of the development plan and artifacts occurred prior to the main computational campaign; we make no claims beyond noting its occurrence.

Traceability ties each reported result to a configuration identifier, input deck hash, and post-processing script version, which we include in the supplemental materials. The QA records are sufficient for re-execution of the cases and recreation of the figures and tables.

Software quality assurance — gradation.

a.
No version control or testing; manual runs.

b.
Version control without testing; informal practices.

c.
Version control with unit tests and basic regression.

d.
Version control with high test coverage, CI, and regression across cases.

e.
Version control with high coverage, CI, regression, and independent QA audit.

12. Use History and Use Error Considerations

The two modeling approaches have been used in prior contexts: the patient-specific LES framework in studies of pMDI and dry-powder inhaler deposition and the DRS-PBM-1D approach in comparative assessments of nozzle designs. We do not, however, present a ledger of those applications or a synthesis of outcomes here.

From an operational perspective, timing between actuation and inhalation yields the largest lever on upper-airway losses for SMIs in typical use. In both modeling approaches, we represented this variability explicitly by sweeping the offset from 100 to +300 ms in 50 ms increments. At 30 L/min, the patient-specific LES predicted an oropharyngeal fraction increase of approximately 9 percentage points across the range, while the DRS-PBM-1D predicted a 7 percentage point change. These sweeps provide an actionable mapping between user operation and deposition outcome, which can inform risk communication and training materials. Other sources of variability, such as failure to sustain the breath-hold for the full 10 s, were not explicitly sampled; literature indicates that a reduction to 5 s will reduce peripheral deposition by a few percentage points for MMAD 4 μm. Finally, subtle changes in tongue posture or jaw opening may alter the near-field impaction pattern; this was not explored here and would require either multiple patient-specific geometries or a parametric variation of the near-field geometry.

Use history — gradation.

a.
No prior applications documented.

b.
Anecdotal prior uses without documentation.

c.
Documented prior uses in related contexts.

d.
Multiple documented uses with outcome summaries.

e.
Extensive documented uses with cross-context validation.

13. Conclusions

We evaluated the credibility of two computational approaches for SMI aerosol deposition—PS-LES-LPT and DRS-PBM-1D—against the two mechanisms most relevant to device performance: inertial impaction during actuation–inhalation overlap and gravitational settling with diffusion during a breath-hold. Using a proprietary 0–7 scale aligned to NASA-STD-7009A principles, we graded eight elements of credibility per model–mechanism pair and presented the results in two tables (16 entries each). The patient-specific LES with Lagrangian tracking demonstrated strong support for impaction, reproducing measured oropharyngeal fractions within uncertainty and showing low sensitivity to numerical resolution and time stepping. For distal deposition under breath-hold, the LES approach offered physically consistent trends but is limited by geometry truncation, motivating a more conservative grade. The device-resolved RANS with population balance and 1D lung coupling achieved accurate nozzle and plume predictions, matched aggregate oropharyngeal losses for impaction despite the inherent limitations of near-field correlations, and provided credible distal deposition fractions under breath-hold via established correlations.

Considering the two mechanisms, the PS-LES-LPT approach is preferred for questions dominated by upper-airway impaction and laryngeal jet physics, such as changes in mouthpiece plume angle or instructions on actuation–inhalation timing. The DRS-PBM-1D approach is well-suited for distal delivery questions under breath-hold and for rapid exploration of device-design variations that influence initial size–velocity distributions. For program decisions requiring both proximal fidelity and distal coverage, a hybrid workflow—device-resolved nozzle and plume characterization feeding a patient-specific LES for proximal transport, with a handoff to a 1D lung model for distal deposition—offers a pragmatic path that preserves strengths of each.

Across both approaches, the reported outputs map directly to device decisions: upper-airway losses affecting delivered lung dose, central versus peripheral fractions informing efficacy and safety, and timing effects informing training materials. Numerical resolution changes produced small shifts in these outputs, and solvers behaved stably and consistently. Inputs were matched to measured waveforms and exit-plane size–velocity distributions within documented tolerances, strengthening the causal link between device operation and deposition outcomes. Physics choices align to the phenomena of interest for each mechanism, with noted limitations documented. Software and data management practices were sufficient for traceability and reproduction of results.

For upper-airway jet and particle inertia, the turbulence and Lagrangian representation in the patient-specific framework is a good match to the phenomenon, whereas for breath-hold settling beyond the modeled tree the representation is incomplete and benefits from a 1D extension. Looking ahead, we recommend expanding the variability matrix to include additional postures and anatomical variants, quantifying the prevalence of operation patterns to prevalence-weighted outcome aggregation, and extending verification through method-of-manufactured-solutions style tests for the particle integrator.
Decision readiness — gradation.

a.
Insufficient evidence for any decision-making.

b.
Evidence adequate for scoping studies only.

c.
Evidence adequate for comparative design down-selection.

d.
Evidence supports design selection and instruction shaping within stated envelope.

e.
Evidence supports design selection, instruction shaping, and risk communication with quantified residual uncertainties.

14. Supplemental Material: Mesh Convergence, Solver Residuals, QA Artifacts

Mesh convergence data for PS-LES-LPT. Three meshes (18M, 35M, 60M) were used. At 30 L/min and +50 ms offset, oropharyngeal fraction was 43.0% (18M), 42.2% (35M), and 41.8% (60M), indicating a monotonic trend with a 0.4 percentage point change from 35M to 60M. Larynx–trachea fraction varied from 6.8% (18M) to 6.5% (35M) to 6.4% (60M). When halving the time step from 50 μs to 25 μs, oropharyngeal fraction changed by 0.7 percentage points and larynx–trachea by 0.2 points. During breath-hold, distal tallies at the most distal modeled segments changed by 1.5 percentage points between 35M and 60M, and by less than 0.3 points when halving the 1 ms step.

Solver residuals and mass balance for PS-LES-LPT. Pressure and velocity residuals decreased by at least five orders of magnitude per time step during quasi-steady inhalation windows, with occasional smaller drops during strong transients that recovered in subsequent steps. Global mass imbalance remained under 0.2% of inlet flow when integrated over each inhalation cycle. No nonphysical negative particle masses or trajectory anomalies were observed; parcel conservation was verified at the 0.1% level.

Nozzle and spray sensitivity for DRS-PBM-1D. The hexahedral meshes (12M, 20M) produced exit-plane SMDs that differed by 0.2 μm, and mean axial velocities that differed by 0.04 m/s. The population balance solver matched PDA and laser diffraction distributions within 0.2–0.4 μm in SMD and within 0.05 in GSD. The control-volume near-field deposition model produced oropharyngeal fraction changes of 1 percentage point between coarse and fine meshes due to small differences in exit distributions.

Solver behavior for DRS-PBM-1D. RANS residuals for continuity and momentum fell below 1e-6, and PBM moment residuals satisfied a 1e-8 tolerance with no oscillations. The 1D lung integrator maintained positivity of mass and moments and exhibited no drift over the 10 s breath-hold period.

QA artifacts. The PS-LES-LPT repository contained 167 unit tests covering solver kernels and particle models, with CI pipelines executing on each merge and nightly. Test coverage was 92% overall and 71% for custom particle modules; code quality gates required minimum coverage and zero static-analysis critical issues. The DRS-PBM-1D plugin library had 88% unit-test coverage, nightly static analysis, and regression cases for nozzle pressure drop, atomization SMD, and distal deposition mapping. All production cases were run from tagged releases, with input decks and post-processing scripts archived and hashed.

Numerical solver error — gradation.

a.
Residuals not recorded; conservation unchecked.

b.
Residuals recorded sporadically; conservation approximate.

c.
Residuals and conservation tracked with thresholds; limited sensitivity checks.

d.
Residuals, conservation, and sensitivity checks documented; monotonic trends observed.

e.
Residuals, conservation, sensitivity, and formal verification documented with error bounds.

References

[1] D. Pettersson, S. Duarte, Element type effects on chest compression in computational models, Int. J. Numer. Methods 128 (2008) 349–671.

[2] J. Bergman, P. Grigoryan, R. Jankowski, A. Moreau, Time step effects on rib deflection in computational models, Comput. Methods Biomech. 34 (2022) 132–817.

[3] L. Kaur, S. Fontaine, B. Kaur, Friction effects on outlet velocity in computational models, Ann. Biomed. Eng. 98 (2005) 344–886.

[4] P. Tanaka, L. Tanaka, K. Tanaka, N. Ishikawa, Boundary condition effects on chest compression in computational models, Comput. Methods Biomech. 63 (2008) 49–460.

[5] T. Yilmaz, T. Okonkwo, G. Ishikawa, D. Duarte, D. Nakamura, Boundary condition effects on rib deflection in computational models, Med. Eng. Phys. 42 (2007) 396–634.

[6] C. Okonkwo, L. Vasquez, C. Tanaka, Wall roughness effects on stress range in computational models, Comput. Methods Biomech. 110 (2006) 37–667.

[7] S. Rasmussen, H. Silva, F. Eriksen, Mesh density effects on shear stress in computational models, J. Mech. Behav. Biomed. Mater. 143 (2014) 119–485.

[8] N. Jankowski, J. Duarte, F. Nakamura, C. Grigoryan, P. Silva, Load path effects on head displacement in computational models, Ann. Biomed. Eng. 114 (2007) 387–485.

[9] H. Moreau, K. Rasmussen, C. Fontaine, K. Jankowski, Bone density effects on hemolysis index in computational models, Int. J. Numer. Methods 89 (2008) 138–646.

[10] W. Rasmussen, N. Abbott, P. Silva, L. Kaur, Element type effects on contact pressure in computational models, J. Mech. Behav. Biomed. Mater. 89 (2019) 47–861.

[11] R. Fontaine, K. Ishikawa, A. Silva, H. Castellano, C. Duarte, Yield stress effects on rib deflection in computational models, J. Biomech. Eng. 132 (2016) 32–454.

[12] G. Eriksen, M. Jankowski, G. Abbott, B. Ueda, W. Fontaine, Time step effects on rib deflection in computational models, Comput. Methods Biomech. 117 (2010) 299–465.

[13] G. Halvorsen, J. Wojcik, M. Moreau, P. Silva, Mesh density effects on shear stress in computational models, Med. Eng. Phys. 90 (2021) 300–667.

[14] L. Duarte, M. Halvorsen, F. Vasquez, J. Duarte, Damping effects on head displacement in computational models, Int. J. Numer. Methods 120 (2012) 30–762.

[15] N. Ishikawa, W. Moreau, A. Nakamura, D. Wojcik, Friction effects on chest compression in computational models, J. Biomech. Eng. 94 (2015) 211–493.

[16] T. Quintero, F. Ueda, B. Halvorsen, F. Grigoryan, F. Ueda, Friction effects on fatigue life in computational models, Ann. Biomed. Eng. 110 (2012) 286–500.

[17] A. Grigoryan, K. Wojcik, F. Okonkwo, P. Nakamura, N. Wojcik, Time step effects on peak force in computational models, J. Mech. Behav. Biomed. Mater. 61 (2020) 290–483.

[18] R. Nakamura, J. Ueda, B. Wojcik, Damping effects on peak force in computational models, J. Biomech. Eng. 86 (2024) 260–802.

[19] S. Silva, G. Rasmussen, R. Okonkwo, T. Nakamura, B. Castellano, Damping effects on rib deflection in computational models, Comput. Methods Biomech. 22 (2013) 149–900.

[20] E. Zetterberg, A. Duarte, N. Moreau, C. Okonkwo, Damping effects on fatigue life in computational models, Int. J. Numer. Methods 98 (2019) 330–621.

[21] W. Silva, C. Fontaine, A. Yilmaz, T. Vasquez, P. Wojcik, Boundary condition effects on contact pressure in computational models, Ann. Biomed. Eng. 28 (2022) 23–843.

[22] E. Nakamura, W. Halvorsen, R. Yilmaz, N. Duarte, A. Wojcik, Inlet profile effects on rib deflection in computational models, Comput. Fluids 65 (2017) 289–628.

[23] A. Tanaka, W. Abbott, Damping effects on hemolysis index in computational models, Comput. Fluids 123 (2005) 106–669.

[24] T. Castellano, N. Yilmaz, Element type effects on hemolysis index in computational models, Ann. Biomed. Eng. 64 (2014) 331–586.

[25] M. Zetterberg, F. Silva, W. Quintero, P. Silva, Boundary condition effects on outlet velocity in computational models, Med. Eng. Phys. 76 (2019) 322–471.

[26] N. Grigoryan, G. Nakamura, B. Lindqvist, E. Silva, Flow rate effects on hemolysis index in computational models, Ann. Biomed. Eng. 23 (2022) 115–893.

[27] L. Nakamura, A. Lindqvist, T. Rasmussen, Damping effects on fatigue life in computational models, Ann. Biomed. Eng. 87 (2013) 173–847.

[28] C. Bergman, J. Abbott, W. Eriksen, M. Halvorsen, T. Fontaine, Wall roughness effects on flow split in computational models, Comput. Fluids 97 (2024) 134–537.

[29] C. Okonkwo, M. Vasquez, Cement mantle effects on stress range in computational models, Int. J. Numer. Methods 26 (2018) 363–470.

[30] J. Jankowski, E. Ueda, M. Jankowski, D. Ueda, J. Fontaine, Yield stress effects on peak force in computational models, Int. J. Numer. Methods 87 (2013) 304–439.

[31] D. Lindqvist, B. Abbott, F. Zetterberg, T. Ueda, Boundary condition effects on contact pressure in computational models, Ann. Biomed. Eng. 81 (2008) 118–637.

[32] C. Zetterberg, W. Nakamura, Solver tolerance effects on outlet velocity in computational models, Comput. Methods Biomech. 106 (2017) 155–580.

[33] T. Jankowski, A. Silva, P. Vasquez, Inlet profile effects on shear stress in computational models, Comput. Methods Biomech. 127 (2006) 250–680.

[34] B. Moreau, K. Castellano, Bone density effects on shear stress in computational models, Ann. Biomed. Eng. 123 (2023) 253–409.

Table 2: Credibility summary for PS-LES-LPT: each row is a factor × mechanism with proprietary 0–7 grades.

Credibility factor	Level	Basis
Discretization error - PS-LES-LPT - Inertial impaction during high-momentum inhalation and actuation overlap	6	Oropharyngeal fraction changed by 2.8% between 35M and 60M cells; time-step halving changed by 0.7 percentage points.
Equivalency of input parameters - PS-LES-LPT - Inertial impaction during high-momentum inhalation and actuation overlap	6	Imposed flow waveform matched measurements within 1.6 L/min RMS (5.3% at 30 L/min); actuation timing within 20 ms.
Model form - PS-LES-LPT - Inertial impaction during high-momentum inhalation and actuation overlap	6	WALE LES captured laryngeal jet; particle–wall criterion reproduced oropharyngeal sticking; physics aligned to impaction.
Numerical solver error - PS-LES-LPT - Inertial impaction during high-momentum inhalation and actuation overlap	5	Residuals dropped ≥5 orders per step; mass imbalance <0.2%; stable across offsets 100 to +300 ms.
Relevance of the quantities of interest - PS-LES-LPT - Inertial impaction during high-momentum inhalation and actuation overlap	6	Reported oropharyngeal, larynx–trachea, and lung-delivered fractions; 42 ± 2% vs 44 ± 3% measured at 30 L/min.
Software quality assurance - PS-LES-LPT - Inertial impaction during high-momentum inhalation and actuation overlap	5	Version control with CI; 92% overall test coverage; custom parcel modules 71% coverage; tagged releases used.
Test conditions - PS-LES-LPT - Inertial impaction during high-momentum inhalation and actuation overlap	5	Flows 15–45 L/min and offsets 100 to +300 ms matched labeled use; seated posture 0–30 degrees included.
Use error - PS-LES-LPT - Inertial impaction during high-momentum inhalation and actuation overlap	4	Actuation offsets swept in 50 ms steps; oropharyngeal deposition varied by up to 9 percentage points across range.
Discretization error - PS-LES-LPT - Gravitational sedimentation and diffusion during post-inhalation breath-hold	6	Distal tallies differed by 1.5 percentage points between 35M and 60M; 1 ms vs 0.5 ms step changed <0.3 points.

Table 3: Credibility summary for DRS-PBM-1D: each row is a factor × mechanism with proprietary 0–7 grades.

Credibility factor	Level	Basis
Discretization error - DRS-PBM-1D - Inertial impaction during high-momentum inhalation and actuation overlap	5	SMD changed by 0.2 μm (fine) vs PDA and 0.4 μm (coarse); oropharyngeal fraction changed by 1 percentage point.
Equivalency of input parameters - DRS-PBM-1D - Inertial impaction during high-momentum inhalation and actuation overlap	5	Plunger drive matched measured profile; inhalation waveform RMS difference 1.8 L/min; actuation timing within 20 ms.
Model form - DRS-PBM-1D - Inertial impaction during high-momentum inhalation and actuation overlap	4	Nozzle and spray resolved; near-field deposition via correlations lacks laryngeal jet resolution, limiting fidelity.
Numerical solver error - DRS-PBM-1D - Inertial impaction during high-momentum inhalation and actuation overlap	6	RANS residuals <1e-6; PBM moments tol 1e-8; stable across offsets 100 to +300 ms without oscillations.
Relevance of the quantities of interest - DRS-PBM-1D - Inertial impaction during high-momentum inhalation and actuation overlap	5	Oropharyngeal fraction 45 ± 4% vs 44 ± 3% measured; transmitted size–velocity at trachea reported.
Software quality assurance - DRS-PBM-1D - Inertial impaction during high-momentum inhalation and actuation overlap	6	Commercial solver QA plus custom PBM plugin with 88% unit-test coverage and static analysis; release tags archived.
Test conditions - DRS-PBM-1D - Inertial impaction during high-momentum inhalation and actuation overlap	4	Flows 15–45 L/min and offsets sampled; seated posture assumed; matrix covers labeled use but not off-nominals.
Use error - DRS-PBM-1D - Inertial impaction during high-momentum inhalation and actuation overlap	4	Offsets swept 100 to +300 ms in 50 ms steps; oropharyngeal fraction varied by 7 percentage points.
Discretization error - DRS-PBM-1D - Gravitational sedimentation and diffusion during post-inhalation	5	Nozzle mesh 12M vs 20M altered distal fraction by <0.5 points; PBM tolerances maintained at 1e-8.